Materials Research Bulletin 184 (2025) 113260

Contents lists available at ScienceDirect

Materials Research Bulletin

journal homepage: www.elsevier.com/locate/matresbu

Research papers

Analytical modeling and performance enhancement of Cu(In,Ga)Se_2 chalcopyrite solar cells through nanostructure integration

Nassima El Ouarie [a,b], Jawad El Hamdaoui [c], Asmae El Aouami [b], Mohamed El-Yadri [b], Girija Shankar Sahoo [d], Karina G. Rodriguez-Osorio [e], Maykel Courel [e], Laura M. Pérez [f], Pablo Díaz [g], David Laroze [h], Vijay Karade [i], Abdelouahed El Fatimy [c], El Mustapha Feddi [c,b,*]

[a] Laboratory of Condensed Matter and Interdisciplinary Sciences (LaMCScI), Faculty of Sciences Rabat, Mohammed V University in Rabat, Morocco
[b] Group of Optoelectronic of Semiconductors and Nanomaterials, ENSAM, Mohammed V University in Rabat, Morocco
[c] School of Applied and Engineering Physics, Mohammed VI Polytechnic University, Lot 660, Hay Moulay Rachid Ben Guerir, 43150, Morocco
[d] School of Electronics Engineering (SENSE), Vellore Institute of Technology, Vandalur-Kellambakkam Road, Chennai, Tamil Nadu 600127, India
[e] Centro Universitario de los Valles, Universidad de Guadalajara, Carretera Guadalajara-Ameca, 46600, Ameca, Jalisco, Mexico
[f] Departamento de Ingeniería Industrial y de Sistemas, Universidad de Tarapacá, Casilla 7D, Arica, Chile
[g] Departamento de Ciencias Físicas, Universidad de La Frontera, Casilla 54-D, Temuco, Chile
[h] Instituto de Alta Investigación, Universidad de Tarapacá, Casilla 7 D, Arica 1000000, Chile
[i] Department of Energy Engineering, Korea Institute of Energy Technology (KENTECH), 72, Ujeong-Ro, Naju-Si, Jeollanam-do, South Korea

ARTICLE INFO

Keywords:
Chalcopyrite
CIGSe solar cells
Nanostructures
Quantum wells
Radiative limit

ABSTRACT

$CuGaSe_2$ (CGSe), $CuInSe_2$ (CISe), and Cu (In,Ga)Se_2 (CIGSe) are highly attractive chalcopyrite materials due to their exceptional optoelectronic properties, which make them a suitable candidate for solar cells application. However, highest power conversion efficiency (PCE) reported for these photo absorber materials is close to 20%, which is far below the theoretical limit. It is possible to approach the theoretical limit by incorporating nanostructures into the cell, which initiates the sub-bandgap (E_g) absorption by forming an intermediate band (IB). In this study, CISe nanostructures are incorporated within the CGSe host material to form a CGSe/CISe quantum wells (QWs). This method utilizes the host semiconductor's wider E_g to maintain the open-circuit voltage (V_{oc}) values that are comparable to those reported for CGSe solar cells. The study examines the effects of QWs thickness, QWs number, and Ga/(Ga+In) compositional ratio on the characteristics of solar cells. Results indicate that incorporating 50 QWs with thicknesses ranging from 20 to 150 nm and Ga/(Ga+In) compositional ratios of about 0.2 and 0.8, respectively, can enhance PCE, further highlighting the importance and positivity of nanostructures. In addition, improvements in short-circuit current density, V_{oc}, and overall PCE are also observed than the optimized device without nanostructures. The study proposes a promising approach to improve the photo absorption, carrier separation and thereby over all solar cell performance based on Chalcopyrite heterostructure QWs.

1. Introduction

Recently the Cu(In,Ga)Se_2 (CIGS) based thin films solar cells (TF-SCs) has received tremendous attention due to their fundamental properties: their low cost, easy integration, and high power conversion efficiency [1–3]. Though the Power Conversion Efficiency of CIGS solar cells still lies below theoretical Shockley–Queisser (S–Q) limit. One of the significant challenges that limits the further improvement in CIGS efficiency is the effective use of the solar spectrum. Briefly, the problem with these cells is that they are unable to absorb photons whose energy is below the bandgap (E_g) of the bulk semiconductor. The device's current density would rise, if these photons were absorbed, leading to a boost in efficiency, provided that the voltage output of the cells is not significantly degraded. However, changing the semiconductor E_g alone cannot solve this problem, as narrowing the E_g value leads to an increase in recombination, which degrades the open-circuit voltage (V_{OC}) and thereby the Power Conversion Efficiency [4]. To overcome this issue, finding a new approach that guarantees a higher absorption of photons while minimizing the reduction in V_{OC} is crucial. Enhancing Power Conversion Efficiency can be achieved by integrating nanostructures like quantum wells (QWs) into the bulk material [5].

* Corresponding author at: School of Applied and Engineering Physics, Mohammed VI Polytechnic University, Lot 660, Hay Moulay Rachid Ben Guerir, 43150, Morocco.
E-mail address: e.Feddi@um5r.ac.ma (E. Feddi).

https://doi.org/10.1016/j.materresbull.2024.113260
Received 26 August 2024; Received in revised form 27 November 2024; Accepted 9 December 2024
Available online 16 December 2024

Quantum well solar cells are considered a promising approach for next-generation photovoltaic technology, receiving significant attention from both experimental and theoretical perspectives [5]. Recently, M. Courel et al. proposed an innovative approach to enhance the efficiency of Kesterite solar cells by incorporating quantum well nanostructures, and achieved a remarkable efficiency of 45.8% by varying the compositional ratios [4,6]. Additionally, they reported an 11.1% improvement in SnS cell efficiency with integrating SnSSe nanostructures, attributed to a boost in short-circuit current [7]. Advances in CIGS nanostructures for thin-film solar cells include single-phase chalcopyrite growth with 10% gallium, verified by XRD and UV–Vis spectroscopy [8], and quantum-well-enhanced CIGS cells achieving 24.23% efficiency [9]. Cost-reduction efforts by Yaroslav E. Romanyuk et al. reached 13.8% efficiency using solution-processed CIGS without high-temperature selenization [10]. Light-trapping via nanostructured back mirrors in ultrathin CIGS cells has enabled potential efficiencies of up to 20% [11], while gallium profile studies highlight its impact on recombination mechanisms in CIGS cells [12]. Furthermore, cadmium incorporation in CdS buffer layers improved CIGS efficiency from 11.0% to 15.5% by reducing deep-level defects [13]. These studies emphasize the importance of nanostructure integration and recombination control in advancing chalcopyrite- and CIGS-based solar cells.

The introduction of quantum well solar cells (QWSCs) since 1990 has sparked significant interest in this approach [14]. By introducing quantum wells (QWs), a new mini band forms in the bandgap of the active material [15]. This formation enhances the absorption of photons, particularly in the Infrared (IR) region of the solar spectrum, leading to a more efficient conversion of sunlight into electricity. Notably, this technique has demonstrated an increase in PCE by facilitating the absorption of additional photons with energies below the bulk bandgap (E_g) [14]. The QWs are integrated into a material and form a type I band-alignment, they create discrete energy levels due to quantum confinement [16,17]. This results in the extension of the absorption range of light to lower energies compared to the absorber E_g. By adjusting the width and depth of the QWs, it is possible to optimize the absorption of photons and achieve maximum PCE. When photons are absorbed by QWs, they generate electron–hole pairs at the QW [18]. These pairs can escape to the bulk cell and contribute to additional current with the assistance of an electric field or thermal energy. Moreover, if the V_{OC} of the nanostructured cell is comparable to that of a solar cell made of bulk material, the additional absorption of photons can increase the PCE. However, incorporating QWs may result in increased carrier losses due to the confinement of carriers, which could diminish the V_{OC} output of the solar cell [19]. Exploring the conditions that enable carrier generation to surpass recombination losses is crucial [4]. It is noteworthy that there has been no prior research on implementing quantum wells in chalcopyrite solar cells [5]. Consequently, this study seeks to provide a numerical analysis of how quantum wells affect chalcopyrite solar cells, considering the radiative limit. This approach holds promise for effectively increasing photon absorption and, consequently, enhancing the photocurrent density of solar cells. This enhancement has the potential to exceed the theoretical limit of Thin-Film Solar Cells (TFSCs).

2. Theoretical considerations

This work undertakes the first-ever assessment of incorporating CIGSe quantum wells into CGSe solar cells. The research involves numerical computations of CGSe/CIGSe quantum well solar cells under the radiative limit, which only accounts for band-to-band transitions. Typically, quantum heterostructures are present in the intrinsic region of a p-i-n structure. As a result, it is envisaged that the CIGSe compound will produce intrinsic defects infrequently, making it nearly intrinsic in the absence of doping. A critical first step in assessing whether employing an absorber material in solar cells is feasible is to determine the radiative limit. This limit only takes into account losses from band-to-band transitions. It leaves out losses from surface reflection, bulk and interface defects, and series and shunt resistances [20]. A perfect buffer layer is taken into account when operating within the radiative limit, allowing the majority of photons to be absorbed in the intrinsic region created by CGSe/CIGSe quantum wells. Furthermore, it is assumed that, the photo-generated electron–hole pairs which are not recombined through radiation, contribute to the photocurrent [2,21]. It is important to highlight that the goal of this study is to identify the circumstances that allow for the highest possible efficiency in the suggested QWSCs. The optimal conditions for maximizing the efficiency of CIGSe solar cells are initially analyzed without incorporating nanostructures, serving as a point of reference for comparison. The current–voltage (J–V) characteristics of the solar cell under the radiative limit without nanostructures can be evaluated using the following equation [22]:

$$J = qWn_i^2 B\left[e^{\left(\frac{qV}{KT}\right)} - 1\right] - J_{PH} \tag{1}$$

where q is the charge of electron, W is the thickness of the absorber layer, ni is the intrinsic carrier concentration, and B denotes the radiative coefficient of the CIGSe material. V denotes the terminal voltage; KT is the thermal energy; and J_{PH} denotes the photocurrent density.

It is well-established that solar cells based on hetero-structures exhibit high efficiency. At the boundaries of the intrinsic region, an electric field is established due to the presence of opposing charges on each side of the P and N junctions. Our hypothesis is based on the incorporating multi-QWs into the depletion region. Strictly speaking, in the radiative limit, two fundamental processes occur: photon absorption and carrier recombination (Fig. 1(a)) [4]. By enabling the absorption of photons within a specific energy range, quantum wells facilitate an increase in the short-circuit current density (J_{sc}) compared to conventional solar cells that lack the capability to capture these photons. Notably, recombination and absorption occur between discrete levels. Indeed, the existence of the electric field (F) in the depletion region leads to tilted QWs inducing the well-known confined Stark effect and consequently the electrons and holes levels undergo Stark shift [23]. In this region, the internal electric field F will be directed along the Z-direction. The energies of the electron and hole are determined by solving the Schrödinger equation, expressed as follows [18]:

$$H\Psi(z) = E\Psi(z) \tag{2}$$

Within the context of the effective mass approximation and the content (x) dependent Hamiltonian for a single particle contained in a CISe/CGSe QW, it can be expressed as follows:

$$H = \frac{-\hbar^2}{2}\frac{\partial}{\partial z}\left(\frac{1}{m_j^*(z)}\frac{\partial}{\partial z}\right) + V_j(z) + |q|\,Fz \quad \text{j= e and h} \tag{3}$$

In Eq. (3), The initial terms signify the kinetic energies, the subsequent terms depict the confinement potential, and the final term describes the dipolar electrostatic energy.

The potential profile of the QW is given by [24]:

$$V_j(z) = \begin{cases} 0 & \text{for } |z| < L/2 \\ V_{0j} & \text{for } |z| \geq L/2 \end{cases} \quad \text{j= e and h} \tag{4}$$

Where the valance band offset for electron and hole are 0.60 eV and 0.04 eV respectively. The effective masses of the charge carrier is found by the following equations:

$$m_j^* = \begin{cases} m_j^*(CISe) & \text{for } |z| < L/2 \\ m_j^*(CGSe) & \text{for } |z| \geq L/2 \end{cases} \quad \text{j= e and h} \tag{5}$$

In the absence of an electric field ($F = 0$), the ground state energy can be determined by solving the Schrödinger equation, considering the resulting equation from the application of Ben-Daniel–Duke boundary conditions [17,18]:

$$\left[\Psi_{well}(z)\right]_{z=\pm L/2} = \left[\Psi_{barrier}(z)\right]_{z=\pm L/2} \tag{6}$$

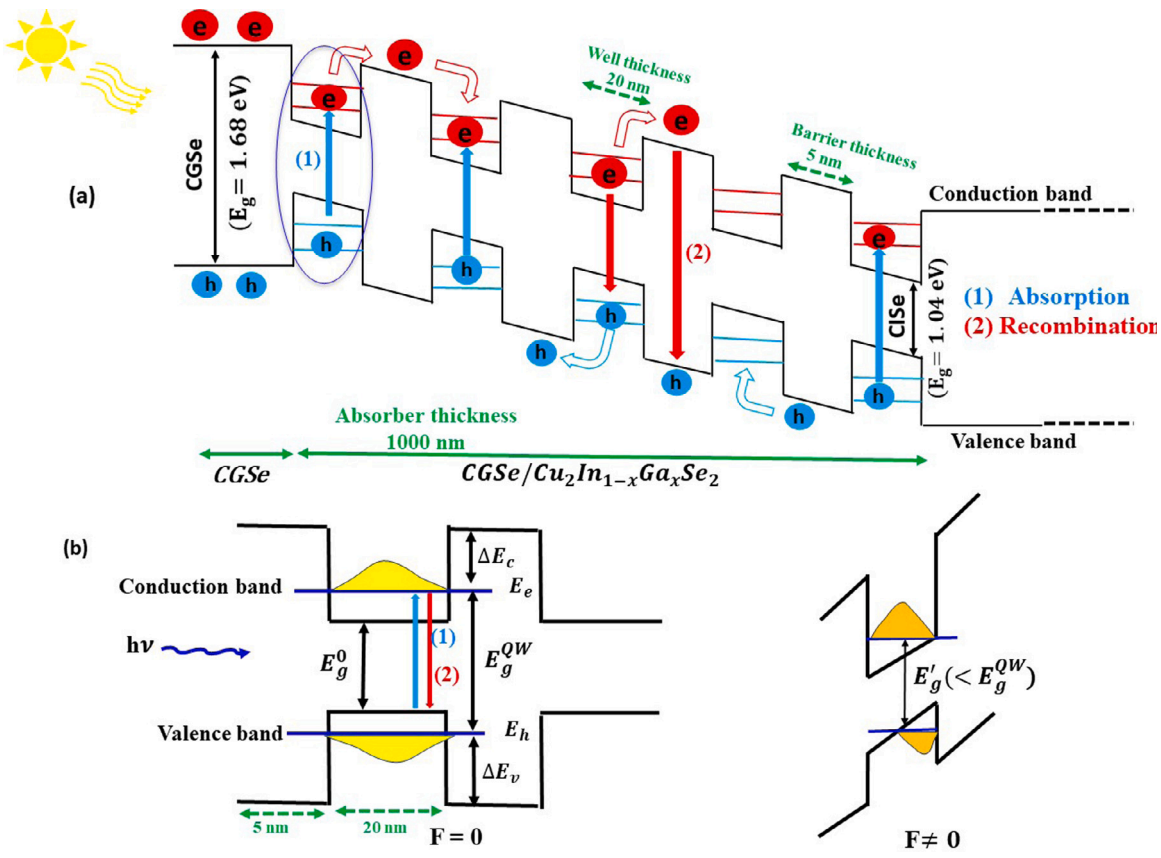

Fig. 1. (a) Schematic of $Cu_2GaSe_2/Cu_2In_{1-x}Ga_xSe_2$ structure and different physical processes. (b) Different energy transitions and band gap modification caused by quantum Confined Stark Effect.

$$\left[\frac{1}{m_j^*(CISe)}\cdot\frac{d\Psi(z)}{dz}\right]_{\pm L/2}=\left[\frac{1}{m_j^*(CGSe)}\cdot\frac{d\Psi(z)}{dz}\right]_{\pm L/2} \tag{7}$$

A transcendental equation is created by combining the two previous equations [23]:

$$tan\left(\frac{m_j^*(CISe)E(z)L^2}{2\hbar^2}\right)^{1/2}=\left(\frac{m_j^*(CISe)}{m_j^*(CGSe)}\left(\frac{V_j-E(z)}{E(z)}\right)\right)^{1/2} \tag{8}$$

The single-particle energy state, designated as $E(z)$, can be found by solving the equation above.

We analytically solved Schrödinger's Eq. (3) using the method proposed by Ghatak et al. [17,25]. in their 1990 work. This allowed us to obtain the wave function and energy values for cases where $(F \neq 0)$. Initially, we performed a transformation of the variable z into a dimensionless coordinate ξ, expressed as:

$$\xi=-\left[\frac{2m_j^*}{(qF\hbar)^2}\right]^{\frac{1}{3}}(E-V_j(z)-|q|\,Fz) \tag{9}$$

Using this variable, we can represent the Schrödinger equation as follows:

$$\frac{d^2\psi(\xi)}{d\xi^2}-\xi\psi(\xi)=0 \tag{10}$$

The wave functions expressed in reference to this transformed coordinate ξ are produced by the superposition of the Airy functions $Ai(\xi)$ and $Bi(\xi)$:

$$\psi(\xi)=\begin{cases}C_1Ai(\xi_1)+D_1Bi(\xi_1) & \text{for } z<-L/2\\ C_2Ai(\xi_2)+D_2Bi(\xi_2) & \text{for } |z|<L/2\\ C_3Ai(\xi_1)+D_3Bi(\xi_1) & \text{for } z>L/2\end{cases} \tag{11}$$

Where C_1, C_2, C_3, D_1, D_2 and D_3 are constants. The expressions of ξ_1(for $|z| > L/2$) and ξ_2(for $|z| < L/2$) are :

$$\begin{aligned}\xi_1&=-\left[\frac{2m_j^*(CGSe)}{(qF\hbar)^2}\right]^{\frac{1}{3}}(E-V_{0j}-|q|\,Fz)\\ \xi_2&=-\left[\frac{2m_j^*(CISe)}{(qF\hbar)^2}\right]^{\frac{1}{3}}(E-|q|\,Fz)\end{aligned} \tag{12}$$

The coefficient D_3 must equal 0 since the Airy function Bi tends to infinity as ξ gets closer to infinity. For the sake of simplicity, we can fix C_3 to 1 without compromising the generality of the wave function $\Psi(\xi)$, which can be regarded as arbitrary up to a multiplicative constant. By ensuring the continuity of the wave function and its derivative at $z = L/2$, we can determine C_2 and D_2 as follows:

$$C_2=\pi\left[Ai(\xi_{1+})Bi'(\xi_{2+})-\frac{m_j^*(CIS)}{m_j^*(CGS)}Ai'(\xi_{1+})Bi(\xi_{2+})\right] \tag{13}$$

and

$$D_2=\pi\left[\frac{m_j^*(CISe)}{m_j^*(CGSe)}Ai'(\xi_{1+})Ai(\xi_{2+})-Ai(\xi_{1+})Ai'(\xi_{2+})\right] \tag{14}$$

We may determine the values of C_1 and D_1 by using the same boundary conditions at $z = -L/2$ and doing as follows:

$$\begin{aligned}C_1=\pi[&(C_2Ai(\xi_{2-})+D_2Bi(\xi_{2-}))Bi'(\xi_{1-})\\ &-\frac{m_j^*(CGSe)}{m_j^*(CISe)}(C_2Ai'(\xi_{2-}))+D_2Bi'(\xi_{2-})Bi(\xi_{1-})]\end{aligned} \tag{15}$$

and

$$\begin{aligned}D_1=\pi\Bigg[&\frac{m_j^*(CGSe)}{m_j^*(CISe)}(C_2Ai'(\xi_{2-})+D_2Bi'(\xi_{2-}))Ai(\xi_{1-})\\ &-(C_2Ai(\xi_{2-})+D_2Bi(\xi_{2-}))Ai'(\xi_{1-})\ ]\end{aligned} \tag{16}$$

where $\xi_{1\pm}$ and $\xi_{2\pm}$ are defined for $z = \pm L/2$ by :

$$\xi_{1\pm} = -\left[\frac{2m_j^*(CGSe)}{(qF\hbar)^2}\right]^{\frac{1}{3}}(E - V_{0j} \pm \frac{|q|FL}{2})$$
$$\xi_{2\pm} = -\left[\frac{2m_j^*(CISe)}{(qF\hbar)^2}\right]^{\frac{1}{3}}(E \pm \frac{|q|FL}{2}) \quad (17)$$

The energies corresponding to a particular internal electric field are obtained by finding the roots of the transcendental equation $C_1(E) = 0$.

This valuable information can be utilized to accurately calculate generation and recombination rates, enabling the evaluation of the J-V characteristics of QWSCs under the radiative limit.

3. J–V relation

To determine the J-V characteristics of quantum well solar cells (QWSCs) under the radiative limit, equation [26] is used for evaluation :

$$J = J_0(1 + r_R\beta)\left[e^{(\frac{qV}{KT})} - 1\right] - J_{PH} \quad (18)$$

The equation involves the following parameters; J_0 is the reverse saturation current density, q, which represents the electron charge; V, which is the terminal voltage; kT, which represents the thermal energy; and $\beta = \frac{qB_B W n_{iB}^2}{J_0}$. The equilibrium intrinsic carrier concentration for the barrier material is represented by n_{iB}. The radiative enhancement ratio, r_R, is also a crucial parameter as it indicates the fractional increase in radiative recombination. This parameter can be calculated using the following expression :

$$r_R = 1 + f_w\left[\gamma_B\gamma_{DOS}^2 e^{(\frac{\Delta E_g - qFL_w}{KT})} - 1\right] \quad (19)$$

The absorber area in a quantum well solar cell (QWSC) comprises of quantum wells, denoted by f_w. The difference in the bandgap energy between the barrier E_{gb} and the well E_{gw} gives rise to ΔE_g, with E_{gw} as a function of the Ga/(Ga+In) compositional ratio, expressed as: $E_g^{(CIGS_e)}(x) = (1-x)E_g^{(CIS_e)} + xE_g^{(CGS_e)} - 0.15x(1-x)$ [27]. CISe and CGSe have bandgaps of 1.04 eV for ($x = 0$) and 1.68 eV for ($x = 1$). Important parameters that affect QWSCs are the electric field F and well thickness L_w. Additionally, γ_B, which is the ratio of the radiative recombination coefficients of the wells and barriers, can be calculated as $\gamma_B = \frac{B_w}{B_b}$. The ratio between the effective density of states of the wells and the barriers is given by $\gamma_{DOS} = \frac{g_w}{g_b}$, where g_w is the effective density of states of the well. All these parameters together help in the evaluation of the J-V characteristics of QWSCs under the radiative limit. This is demonstrated by the following equation [28]:

$$J_{QWSC} = qWn_i^2 B\left\{1 + f_w\left[\gamma_b\gamma_{DOC}^2 e^{(\frac{\Delta E_g - qFL_w}{KT})} - 1\right]\right\} \times \left[e^{(\frac{qV}{KT})} - 1\right] - J_{PH} \quad (20)$$

The photocurrent density is as follows:

$$J_{PH} = q\int F(\lambda)\left[1 - e^{(-\alpha_b W - \alpha_w N L_w)}\right] d\lambda \quad (21)$$

F(λ) refers to the number of photons per wavelength taken from the AM1.5 G solar spectrum. N represents the number of QW. α_b [22] and α_w [29,30] are the absorption coefficients of the barrier and QW respectively. The absorption coefficient and effective density of states of the QW material are described using stepped functions, which are based on the eigenvalues that result from solving the Schrödinger Eq. (3). The radiative coefficient in barriers and QWs derived from the balance theory writes as follows [29]:

$$B = \frac{2\pi n_r^2}{C^2h^3n_i^2}\int_{E_1}^{\infty}\frac{\alpha E^2}{e^{(\frac{E}{KT})} - 1} dE \quad (22)$$

h is the Planck's constant; c is light velocity; and E_1 represents either the E_g in the barrier material (E_{gb}) or the effective E_g in the QW materials (E'$_g$) (Fig. 1(b)). The determination coefficient B requires knowledge of the intrinsic carrier concentration n_i and absorption coefficient taking into account the discrete levels in the QWs. n_i is determined by calculating the effective density of states of electron g_e or for hole g_h in the QWs using the procedure outlined by Lade [28].

$$g_{e,h} = \frac{m_{e,h}^* k_b T}{\pi\hbar^2 L_W}\sum_i\left[e^{\left(\frac{-E_{e,h}}{k_bT}\right)} - e^{\left(\frac{-\Delta E_{c,v}}{k_bT}\right)}\right] + g_B\left[2\sqrt{\frac{\Delta E_{c,v}}{\pi k_b T}}e^{\left(\frac{-\Delta E_{c,v}}{k_bT}\right)} - \mathrm{erfc}\sqrt{\frac{\Delta E_{c,v}}{k_bT}}\right] \quad (23)$$

where $E_{e,h}$ represents the energies of discrete levels in the optimal electric field. We note that, in contrast to previous work, we now consider the real value of the E_g defined by the relation $E_g^{(w)} = E_g^{(0)} + E_e + E_h$ taking into account the stark shift. $\Delta E_{c,v}$ is the conduction band offset (CBO) and valence band offset (VBO) for electrons and holes. erfc is the complementary error function. Analogous expressions are obtained for the effective densities of state of the bands of light g_{lhw} and heavy g_{hhw} holes. Then the total effective density of state of the QWs can be expressed as follows:

$$g_w = \sqrt{g_{ew}(g_{hhw} + g_{lhw})} \quad (24)$$

All physical parameters are obtained from relevant literature sources, namely the effective masses [31,32] CBO and VBO [33,34] relative dielectric permittivity [35] and refractive index [36]. The Poisson's equation was employed for standard CIGSe solar cells to calculate the electric field. Following a comprehensive series of calculation tests, we determined the optimal value for the electric field to be $F = 26 \times 10^6$ V/m in all calculations. This choice was made meticulously after conducting an exhaustive analysis to achieve the desired photonic properties for our photovoltaic system. The AM1.5 G solar spectrum 100 mW/cm^2 was considered within the range of 300–1300 nm.

To accurately determine the characteristics of QWSCs, we employed both COMSOL and Maple. Using COMSOL [37], we calculated the energy levels for multiple quantum wells by solving the Schrödinger equation with the finite element method (FEM), considering the effects of the electric field and well thickness.

To validate the numerical simulations obtained with COMSOL, we performed an analytical calculation for a single finite quantum well using Maple within the framework of the effective mass approximation. This step allowed us to optimize the meshing strategy, thereby improving and refining the numerical results obtained through the FEM method for the Schrödinger equation in multiple QWSCs. Moreover, Maple was used to calculate the photonic parameters of the solar cell and analyze their behavior under various conditions.

4. Results and discussions

4.1. Analysis of optimal conditions for CIGSe solar cell efficiency without nanostructures

This study begins by investigating the optimal conditions necessary to enhance the efficiency of Copper Indium Gallium Selenide (CIGSe) solar cells in their conventional configuration, without integrating nanostructures. The primary objective is to examine the effects of parameters influencing performance, such as layer thickness and the Ga/(Ga+In) ratio. To achieve this, the analysis is conducted within the framework of the radiative limit, which serves as a benchmark for the maximum theoretical efficiency that solar cells can attain solely through radiative recombination processes. The results depicted in Fig. 2 demonstrate a positive correlation between the thickness of the CIGSe absorbing layer and the short-circuit current density (J_{SC}). As the thickness increases from 1 μm to 6 μm, J_{SC} rises from approximately 28 mA/cm^2 to a maximum of 33.26 mA/cm^2, with a slight

decline observed beyond 3 μm. Thicker layers enhance light absorption, generating more electron–hole pairs, but gains may diminish due to recombination losses. Optimizing the absorbing layer's thickness is crucial for improving solar cell performance, particularly for a Ga/(Ga+In) compositional ratio of 0.6, where thicker layers improve efficiency by enhancing photon absorption. Nevertheless, increasing the thickness of the CIGSe layer results in a decrease in open-circuit voltage (V_{OC}). In Fig. 2(a), we observe that as the thickness of the CIGSe layer increases from 1 μm to 6 μm, V_{OC} gradually decreases from approximately 1.09 V to 1.04 V. This decrease in V_{OC} with increasing thickness indicates a higher rate of charge carrier recombination. This phenomenon is attributed to the longer path that charge carriers must travel within the thicker absorber layer, increasing the likelihood of recombination before reaching the contact due to more frequent interactions and potential energy losses. Ultimately, this leads to increased recombination within the absorber as thickness grows. Moreover, Fig. 2(c) shows that efficiency significantly increases as the thickness rises from 1 μm to approximately 3 μm, reaching a peak of 30.58% due to enhanced photon absorption, which generates more charge carriers and improves the overall current. However, beyond 3 μm, the efficiency begins to plateau and even slightly decline at thicknesses above 4 μm due to increased carrier recombination within the thicker absorbing layer. This phenomenon highlights the existence of an optimal thickness around 3 μm, where efficiency is maximized by balancing photon absorption and minimizing carrier recombination losses. Fig. 2(d) presents the relationship between the Ga/(Ga+In) compositional ratio, the thickness of the CIGSe ($Cu(In,Ga)Se_2$) absorber layer, and the resulting solar cell efficiency. The red area indicates the highest efficiencies, reaching up to 30.85%, observed at a Ga/(Ga+In) ratio of approximately 0.6 and an absorber thickness of around 4 μm. This combination of parameters optimizes efficiency, approaching the theoretical efficiency limit predicted by the Shockley–Queisser model for chalcopyrite materials (around 33%) [38]. Efficiency increases with thickness up to 4 μm, beyond which it stabilizes, suggesting that further increases in thickness do not significantly enhance efficiency due to saturation in light absorption.

4.2. Impact of optimal electric field and quantum well width on energy states

In the subsequent phase, the impact of the internal optimal electric field on the fundamental energy is investigated. Fig. 3(a) depicts the variation in QWs width and its influence on the energy states of electrons and holes, both in the presence and absence of an optimal electric field. In Fig. 3(b), the Stark effect is illustrated for electrons and holes in relation to the variation in QWs with a fixed parameter barrier thickness of $L_b = 5$ nm and temperature$T = 300$ K.

In Fig. 3(a), our initial analysis of both electron and hole energy levels reveals a clear trend. As the width of the QWs increases, there is a notable reduction in the energies of their fundamental states. Furthermore, it is noteworthy that in the absence of an optimal electric field, the energy levels are higher when compared to the situation where an optimal electric field is applied. It is imperative to underscore that the presence of an optimal electric field results in a simultaneous decrease in the energy levels of both electrons and holes. This phenomenon can be attributed to the confined Stark shift, denoted as $\Delta E = E(0) - E(F)$, which becomes more pronounced as the strength of the optimal electric field intensifies, as illustrated in Fig. 3(b). In the narrow width range of 1 to 5 nm, strong confinement is observed, and the Stark effect ($\Delta E = E(0) - E(F)$) is not prominently evident. However, as the width of the QWs extends from 5 nm to 20 nm, the Stark effect becomes more pronounced, especially for holes, as indicated in Fig. 3(b). Conversely, for electrons, the Stark effect displays lower sensitivity. In brief, the figure effectively illustrates how variations in QWs width and the presence of an optimal electric field impact the energy levels of electrons and holes within a QWs [39]. The findings reveal that wider QWs correspond to lower energy levels, and the Stark effect becomes increasingly significant with the expansion of the QWs width and the intensity of the optimal electric field, particularly for holes. Further, study was carried out considering how the number of CISe QWs affects optoelectronic properties in CGSe solar cells, and it also examined how these QWs influence solar cell efficiency across various Ga/(Ga+In) compositional ratios. The analysis was performed using QWs of 20 nm width, with a Ga/(Ga+In) compositional ratio of 1 at barriers (CGSe), and an absorber thickness of 1000 nm, and the smallest barrier thickness would be 5 nm under these circumstances, as demonstrated in Fig. 1. Based on initial calculations, it appears that there is no coupling effect between the QWs in this structure. Therefore, it can be categorized as multiple QWs instead of a superlattice [20,40].

4.3. Effect of the number of quantum wells on solar cell efficiency for different ratios of Ga/(Ga+In)

The number of quantum wells (QWs) in a solar cell structure is a crucial factor for enhancing photon absorption and optimizing device efficiency. This section examines how variations in the number of QWs influence solar cell efficiency across different Ga/(Ga+In) ratios, offering insights into how optimizing QW configurations can achieve efficiencies beyond conventional limits. As illustrated in Fig. 4, an increased number of quantum wells (QWs) enhances the absorption of photons with energies below the CGSe bandgap (E_g), leading to a higher short-circuit current density (J_{SC}). Specifically, Fig. 4(a) shows the correlation between the number of CISe QWs and J_{SC}, with values increasing from 24 to 38 mA/cm^2 as the number of QWs rises. However, increasing the number of QWs also results in a lower open-circuit voltage (V_{OC}) output, as shown in Fig. 4(b), where V_{OC} decreases from 1.08 to 1.03 V. This reduction in V_{OC} is attributed to an increase in carrier recombination, which is due to the enhanced photogeneration of electron–hole pairs and carrier confinement associated with a higher number of QWs. Furthermore, Fig. 4(c) demonstrates the relationship between solar cell efficiency and the number of QWs, where efficiency improves as the number of QWs increases, reaching a maximum efficiency of 33% with 50 QWs, each with a width of 20 nm. This improvement in efficiency is largely due to the enhanced photon absorption that occurs with the addition of more QWs. Additionally, Fig. 4(d) analyzes the impact of the number of QWs on solar cell efficiency across various Ga/(Ga+In) compositional ratios. For all compositions, an increase in the number of QWs beyond 5 leads to higher solar cell efficiency. The trend of increased efficiency in QW-based solar cells is attributed to the increased likelihood of photon absorption, resulting in a higher overall efficiency for different Ga/(Ga+In) ratios, consistent with results reported for other types of quantum well solar cells (QWSCs) [4,26,41]. Based on these findings, a constant value of 50 QWs will be used in further calculations to optimize efficiency. Our study also highlights the significance of QW thickness as a critical parameter for enhancing solar cell performance, as shown in Fig. 3. Adjusting the thickness of QWs enables control over energy levels and absorption properties, which plays an essential role in the design and optimization of electronic devices. For the necessary calculations, the absorber layer thickness was increased while keeping the barrier thickness constant at 5 nm and using 50 QWs. Notably, without the integration of nanostructures, varying the absorber thickness from 1000 nm to 6 μm would result in a maximum efficiency limit of 30%, as previously demonstrated. Therefore, the incorporation of nanostructures, such as QWs, is essential to achieve efficiencies greater than 30%.

4.4. Impact of quantum well thickness on solar cell efficiency for different ratios of Ga/(Ga+In)

The thickness of quantum wells (QWs) is a crucial parameter that directly impacts the optoelectronic performance of CIGSe solar cells.

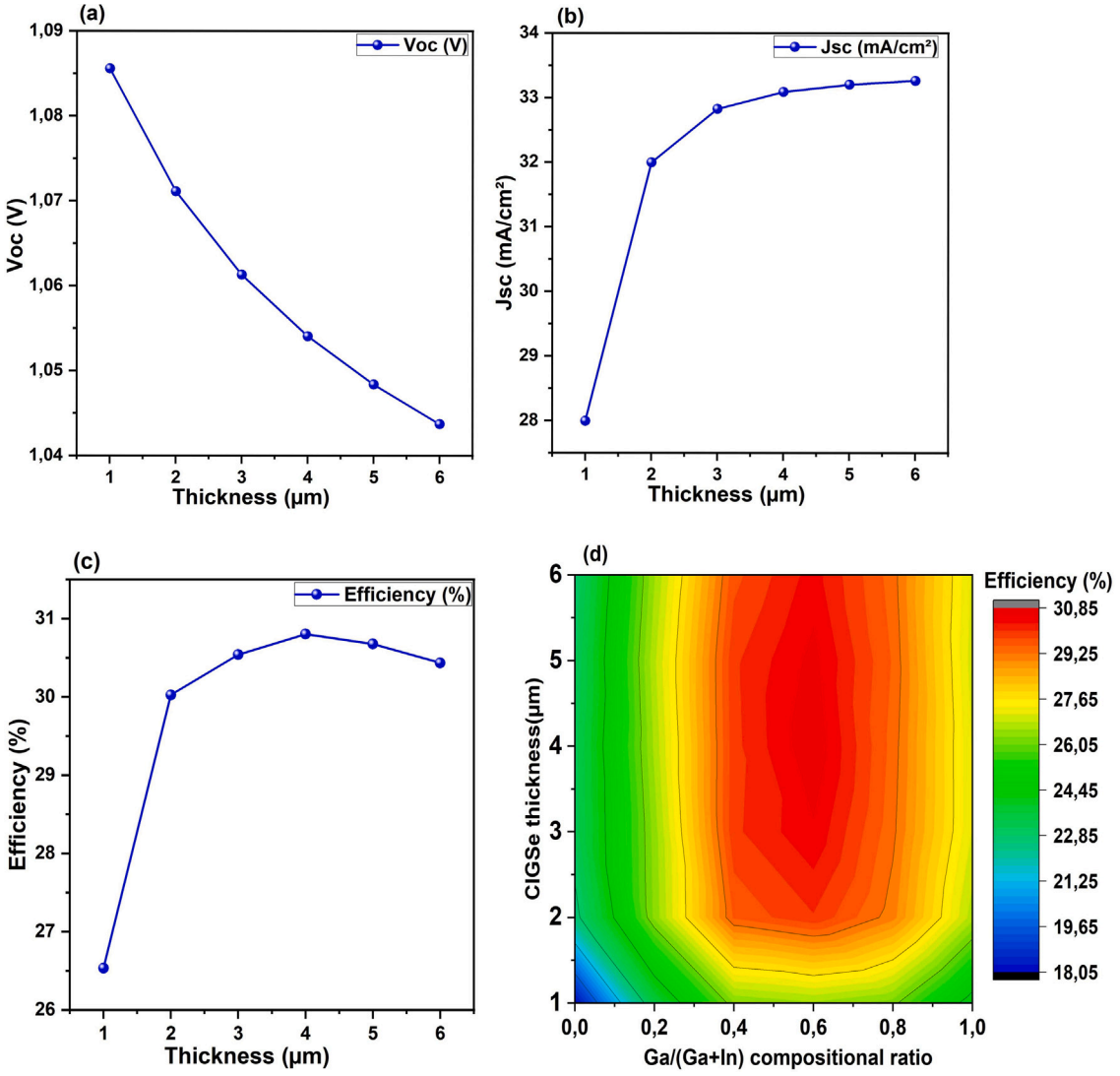

Fig. 2. Influence of CIGSe thickness on J_{SC}, V_{OC}, and overall efficiency with a Ga/(Ga+In) ratio of 0.6, as QW as its efficiency regarding the Ga/(Ga+In) ratio and CIGSe layer thickness.

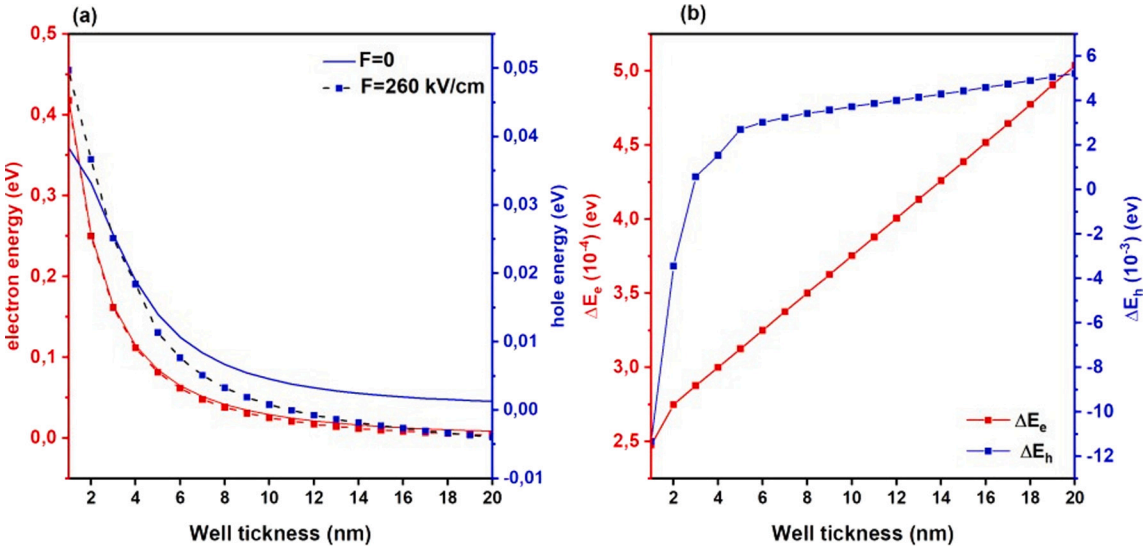

Fig. 3. (a) Variation of electron and hole Energies versus the Lw for an optimal Electric Field. (b) Stark shift for electron and hole versus L_w.

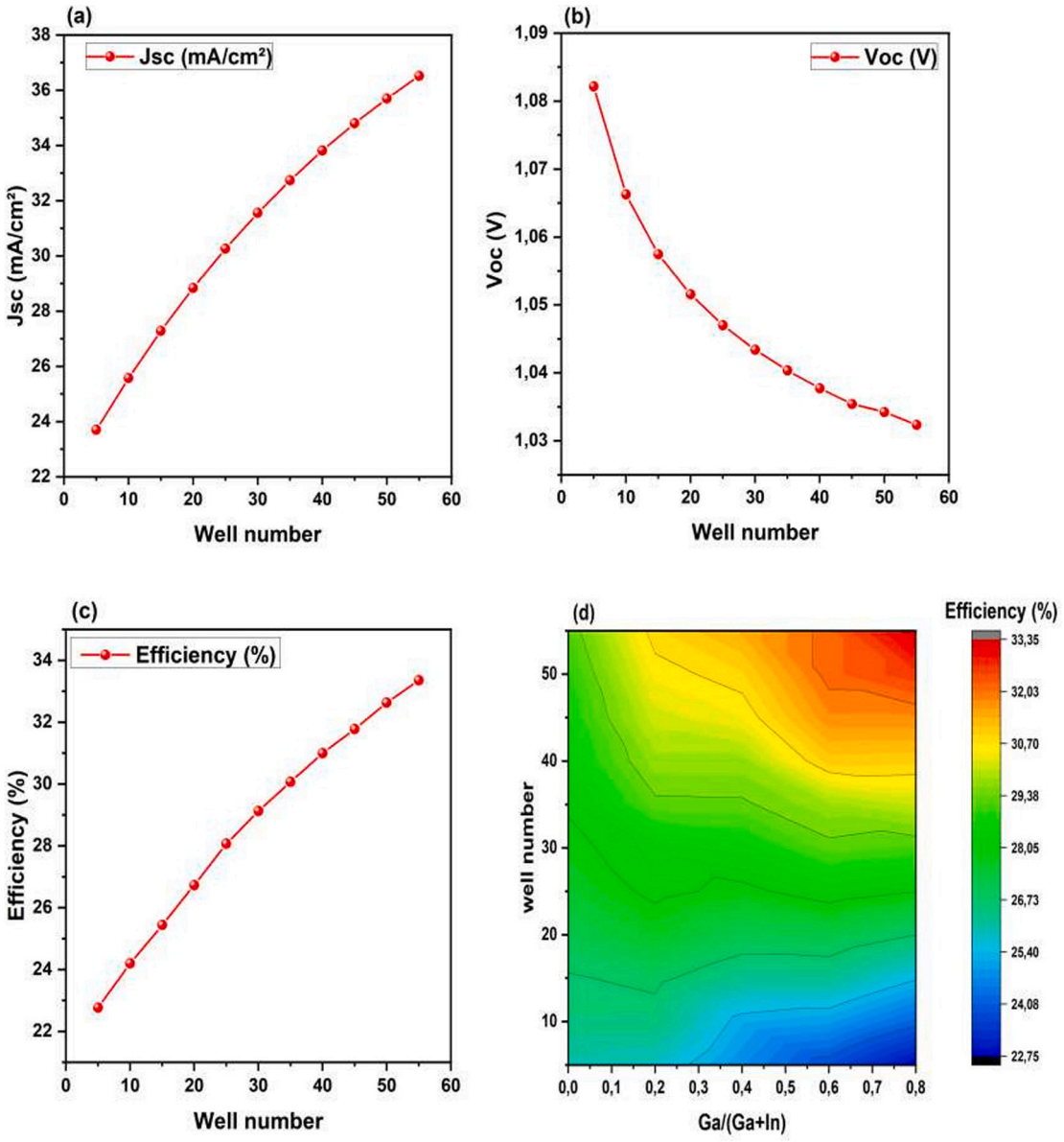

Fig. 4. (a) J_{SC}, (b) V_{OC}, and (c) efficiency in CGSe/CISe solar cells. (d) Efficiency versus the QW number, for different ratios of Ga/(Ga+In).

The results presented in Fig. 5 provide a detailed and compelling analysis of the impact of quantum well (QW) thickness on the key performance parameters of CIGSe solar cells, highlighting effective methods for enhancing their efficiency. Fig. 5(a) shows that increasing the QW thickness from 20 nm to 150 nm leads to a rise in short-circuit current density (J_{SC}) from 35 mA/cm^2 to 38 mA/cm^2. This increase in J_{SC} is attributed to the generation of new energy levels within the QWs and their gradual transition to lower energy states, which improves photon absorption. In contrast, narrow QWs, with photon absorption limited to just a few levels, produce J_{SC} values comparable to conventional CIGSe solar cells without nanostructures. Fig. 5(b) illustrates that increasing the QW thickness also enhances the open-circuit voltage (V_{OC}), a result of reduced carrier recombination. Thicker QWs create more favorable conditions for carriers to escape the wells under the influence of the electric field, effectively minimizing radiative recombination losses and thus improving V_{OC}. This reduction in recombination, as shown in Fig. 5(c), translates into a significant increase in the overall efficiency of the solar cell, which rises from 33% to a maximum of 44% with increasing QW thickness. Additionally, the study investigates the effect of QW composition, particularly the Ga/(Ga+In) ratio, on efficiency for QW thicknesses ranging from 20 to 150 nm, as depicted in Fig. 5(d). The results suggest that deeper QWs, combined with optimized Ga/(Ga+In) ratios of 0.8 and 0 respectively, facilitate easier carrier escape with the electric field's assistance, further reducing radiative recombination losses. An optimized QW thickness of 150 nm is projected to achieve an efficiency of 43.45%, bringing the performance of CIGSe nanostructured cells close to that of two-terminal tandem cells such as perovskite/CIGSe. The optimized solar cell with nanostructures also demonstrates superior J_{SC} and V_{OC} values, achieving 37.31 mA/cm^2 and 1.195 V, respectively, compared to a cell without nanostructures. When compared to CIGSe solar cells lacking nanostructures, the nanostructured variants exhibit similar V_{OC} but a notably higher J_{SC} due to enhanced photon absorption. Overall, these results highlight the effectiveness of incorporating nanostructures into solar cells to optimize performance, making a substantial contribution to advancing photovoltaic technology.

5. Conclusion

Overall, this research highlights the promising prospects of utilizing nanostructures to improve the performance of chalcopyrite solar cells.

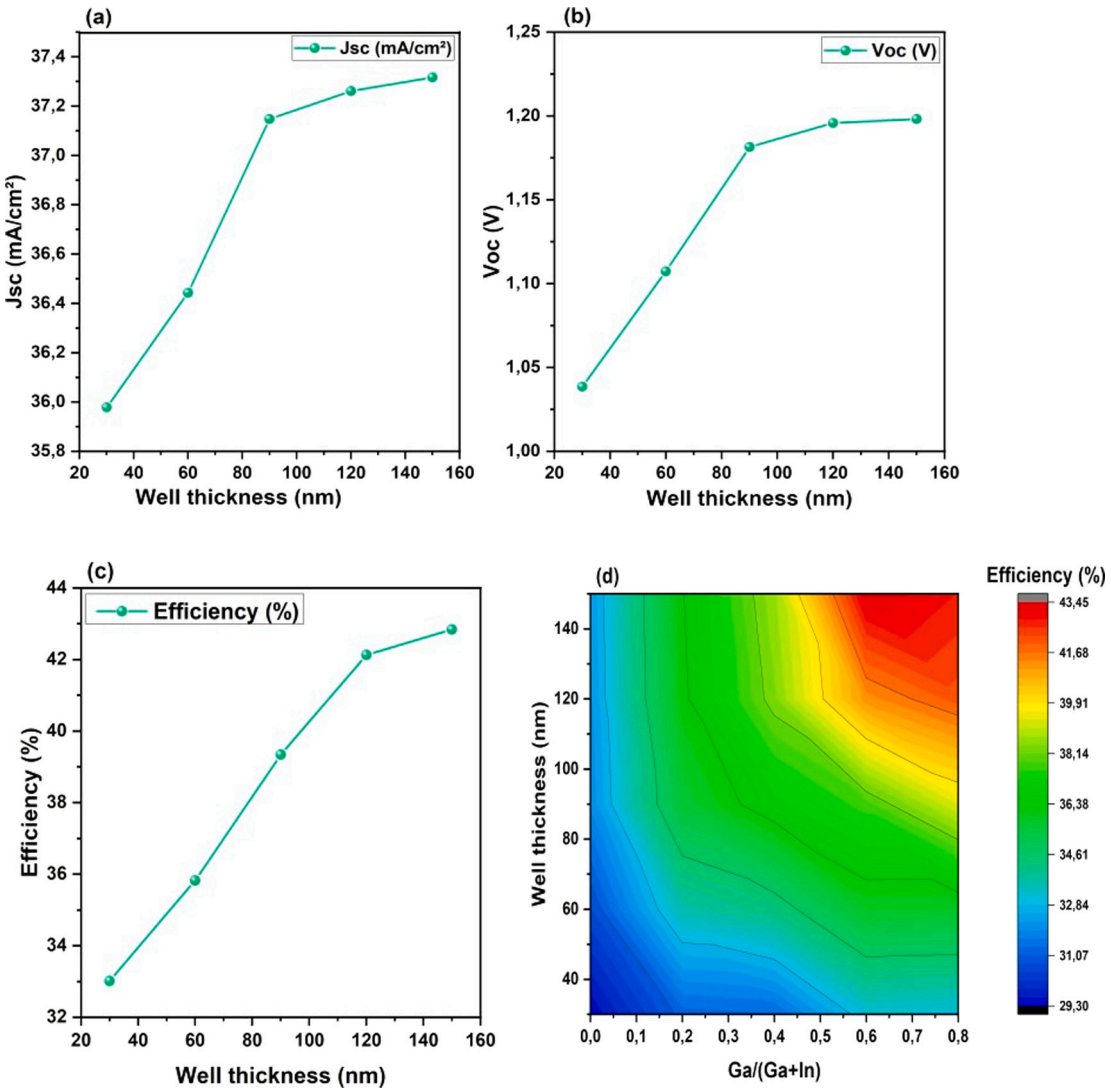

Fig. 5. (a) J_{SC}, (b) V_{OC}, and (c) efficiency in CGSe/CISe solar cells. (d) Efficiency versus the QW thickness, for different ratios of Ga/(Ga+In).

It reveals that the successful implementation of CGSe/CISe nanostructures requires the fulfillment of several crucial conditions to achieve optimal efficiency, as compared to solar cells without nanostructures, as dictated by the radiative limit. First and foremost, a high-quality crystalline chalcopyrite compound with minimal defects and secondary phases is essential for attaining the desired outcomes. Moreover, precise control over the layer thickness and composition within the wells is crucial. Minimizing the defect density at interfaces is also paramount to prevent nonradiative recombination losses. The proposed optimized quantum wells, featuring 50 high-width wells along with 5 nm barriers and specific compositional ratios of 1 to 0.2 for the QWs, ensures high efficiency with the help of two step photo absorption. The optimized solar cell shows an efficiency of 43.45%, with superior J_{SC} and V_{OC} values of 37.31 mA/cm^2 and 1.195 V, respectively. It is worth noting that this study marks the first exploration of incorporating quantum wells in chalcopyrite solar cells, with the potential for future extensions to include quantum dots or other nanostructures, thereby further enhancing solar cell efficiency. However, achieving these advancements necessitates addressing various challenges and continuing scientific investigations in the field.

CRediT authorship contribution statement

Nassima El Ouarie: Writing – original draft, Validation, Methodology, Data curation. **Jawad El Hamdaoui:** Writing – review & editing, Methodology, Investigation. **Asmae El Aouami:** Validation, Software. **Mohamed El-Yadri:** Validation, Software,. **Girija Shankar Sahoo:** Writing – review & editing, Methodology, Investigation. **Karina G. Rodriguez-Osorio:** Methodology, Validation. **Maykel Courel:** Visualization, Validation, Methodology. **Laura M. Pérez:** Writing – review & editing, Validation, Investigation,Software. **Pablo Díaz:** Software, Validation. **David Laroze:** Writing – review & editing, Resources, Project administration, Formal analysis. **Vijay Karade:** Writing – review & editing, Visualization. **Abdelouahed El Fatimy:** Writing – review & editing, Validation, Project administration, Methodology. **El Mustapha Feddi:** Conceptualization, Validation, Supervision, Project administration,.

Declaration of competing interest

The authors confirm that they do not have any conflict of interest in connection with this investigation.

Acknowledgments

LMP acknowledges financial support from ANID through Convocatoria Nacional Subvención a Instalación en la Academia Convocatoria Año 2021, Grant SA77210040. LMP and DL acknowledge partial financial support from ANID through FONDECYT 1240985.

Data availability

No data was used for the research described in the article.

References

[1] M. Contreras, J. Tuttle, D. Du, Y. Qi, A. Swartzlander, A. Tennant, R. Noufi, Appl. Phys. Lett. 63 (1993) 1824.
[2] N. Mufti, T. Amrillah, A. Taufiq, Sunaryono, Aripriharta, M. Diantoro, Zulhadjri, H. Nur, Sol. Energy 207 (2020) 1146.
[3] S. Yang, T. Lin, M. Ochoa, H. Lai, R. Kothandaraman, F. Fu, A. Tiwari, R. Carron, Nat. Energy 8 (2023) 40.
[4] M. Courel, Appl. Phys. Lett. 115 (2019) 123901.
[5] I. Sayed, S. Bedair, IEEE J. Photovolt. 9 (2019).
[6] Karina G. Rodriguez-Osorio, Juan P. Morán-Lázaro, Miguel Ojeda-Martínez, Isaac Montoya De Los Santos, Nassima El Ouarie, El Mustapha Feddi, Laura M. Pérez, David Laroze, Soumyaranjan Routray, Fernando J. Sánchez-Rodríguez, Maykel Courel, Nanomaterials 13 (2023) 2058.
[7] Maykel Courel, P. Beltrán-Bobadilla, F.J. Sánchez-Rodríguez, I. Montoya De Los Santos, M. Ojeda, A. Carrillo-Osuna, Hugo J. Cortina-Marrero, L. Hechavarría-Difur, L.M. Pérez, D. Laroze, E. Feddi, J. Phys. D: Appl. Phys. 54 (2021) 505501.
[8] P. Jakhmola, P.K. Jha, S.P. Bhatnagar, J. Phys. D: Appl. Phys. 6 (2016) 673.
[9] Sina Azizifar, Mohsen Imanieh, Saeid Hassanhosseini, Farhad Bahadori-Jahromi, Opt. Quantum Electron. 52 (2020) 1.
[10] Yaroslav E. Romanyuk, Harald Hagendorfer, Patrick Stücheli, Peter Fuchs, Alexander R. Uhl, Carolin M. Sutter-Fella, Melanie Werner, Stefan Haass, Josua Stückelberger, Cédric Broussillou, Pierre-Philippe Grand, Veronica Bermudez, Ayodhya N. Tiwari, Adv. Funct. Mater. 25 (2015) 12.
[11] Julie Goffard, Clément Colin, Fabien Mollica, Andrea Cattoni, Christophe Sauvan, Philippe Lalanne, Jean-Francois Guillemoles, Negar Naghavi, Stéphane Collin, IEEE J. Photovolt. 7 (2017) 1433.
[12] Jennifer P. Teixeira, Ricardo B.L. Vieira, Bruno P. Falcao, Marika Edoff, Pedro Manuel Parracho Salomé, Joaquim Pratas Leitão, J. Phys. Chem. C 124 (2020) 12295.
[13] Hui Li, Jingwei Chen, Yi Zhang, et al., ACS Appl. Energy Mater. 3 (2020) 9459.
[14] K. Barnham, G. Duggan, Appl. Phys. 67 (1990) 3490.
[15] S. Aazou, E. Assaid, Modelling real photovoltaic solar cell using maple, in: 21st IEEE International Conference on Microelectronics, Marrakech, 2009.
[16] M. Afshar, S. Sadewasser, J. Albert, S. Lehmann, D. Abou-Ras, D.F. Marrón, A. Rockett, E. Räsänen, M. Lux-Steiner, Adv. Energy Mater. 1 (2011) 1109.
[17] A.E. Aouami, M. Bikerouin, M. El-Yadri, E. Feddi, F. Dujardin, M. Courel, B. Chouchen, M. Gazzah, H. Belmabrouk, Sol. Energy 201 (2020) 339.
[18] S. Panda, E. Li, Superlattices Microstruct. 22 (1997) 313.
[19] Keith Barnham, James Connolly, Paul Griffin, Guido Haarpaintner, Jenny Nelson, Ernest Tsui, Alexander Zachariou, Jane Osborne, Chris Button, Geoff Hill, et al., J. Appl. Phys. 80 (1996) 1201.
[20] M. Courel, P. Beltrán-Bobadilla, F. Sánchez-Rodríguez, I.M.D.L. Santos, M. Ojeda, A. Carrillo-Osuna, H. Cortina-Marrero, L.H. Difur, L. Pérez, D. Laroze, E. Feddi, J. Phys. D: Appl. Phys. 54 (2021) 505501.
[21] N.E. Ouarie, J.E. Hamdaoui, G. Sahoo, K. Rodriguez-Osorio, M. Courel, M. Zazoui, L. Pérez, D. Laroze, E. Feddi, Sol. Energy 263 (2023) 111929.
[22] T. Jiménez, D. Seuret-Jiménez, O. Vigil-Galán, M. Basurto-Pensado, M. Courel, J. Phys. D: Appl. Phys. 51 (2018) 435501.
[23] S. Panda, B. Panda, S. Fung, C. Berlin, Phys. Status Solidi (B) 194 (1996) 547.
[24] O.L. Lazarenkova, A.A. Balandin, J. Appl. Phys. 89 (2001) 5509.
[25] A. Ghatak, I. Goyal, R. Gallawa, IEEE J. Quantum Electron. 26 (1990) 305.
[26] J. Rimada, L. Hernández, Microelectron. J. 32 (2001) 719.
[27] D. Valencia, J. Conde, A. Ashok, C. Meza-Avendaño, H. Vilchis, S. Velumani, Sol. Energy 224 (2021) 298.
[28] M. Courel, J. Rimada, L. Hernández, Appl. Phys. 112 (2012) 3054511.
[29] L. Hernández, A. Contreras-Solorio, A. Enciso, C. Cabrera, M. Courel, J. Connolly, J. Rimada, Solar Cells– New Approaches and Reviews, InTech, 2015.
[30] G. Bastard, Wave Mechanics Applied to Semiconductor Heterostructures, Les Editions de Physique, 1988.
[31] S. Siebentritt, M. Igalson, C. Persson, S. Lany, Prog. Photovolt., Res. Appl. 18 (2010) 390.
[32] C. Persson, Appl. Phys. Lett. 93 (2008) 072106.
[33] S.H. Wei, A. Zunger, Appl. Phys. 78 (1995) 3846.
[34] J. Ojajärvi, E. Räsänen, S. Sadewasser, S. Lehmann, P. Wagner, M. Lux-Steiner, Appl. Phys. Lett. 99 (2011) 111907.
[35] A. Adhikari, J.E.C. Diaz, O. Reyes-Vallejo, F.J.G. Cano, M. de la Luz Olvera Amador, V. Subramaniam, Mater. Today Commun. 34 (2023) 105338.
[36] P. Nayebi, K. Mirabbaszadeh, M. Shamshirsaz, Physica B 416 (2013) 55.
[37] Comsol multiphysics modeling software, http://www.comsol.com, license number 2086906.
[38] W. Shockley, H. Queisser, J. Appl. Phys. 32 (1961) 510.
[39] H. Hovel, Semiconductors and Semimetals, Academic Press, New York, San Francisco, London, 1975.
[40] M. Kisin, H. El-Ghoroury, J. Appl. Phys. 107 (2010) 103106.
[41] J. Rimada, L. Hernández, K. Barnham, J. Connolly, Phys. Status Solidi b 242 (2005) 1842.